

# Wavelet decomposition of forced turbulence: applicability of the iterative Donoho-Johnstone threshold

Jesse W. Lord and Mark P. Rast\*

*Laboratory for Atmospheric and Space Physics,  
Department of Astrophysical and Planetary Sciences,  
University of Colorado, Boulder, Colorado*

Christopher Mckinlay<sup>†</sup> and John Clyne

*Computational and Information Systems Laboratory,  
National Center for Atmospheric Research<sup>‡</sup>, Boulder, Colorado*

Pablo D. Mininni<sup>§</sup>

*Departamento de Física, Facultad de Ciencias Exactas y Naturales,  
Universidad de Buenos Aires, Argentina*

(Dated: January 9, 2012)

## Abstract

We examine the decomposition of forced Taylor-Green and Arn'old-Beltrami-Childress (ABC) flows into coherent and incoherent components using an orthonormal wavelet decomposition. We ask whether wavelet coefficient thresholding based on the Donoho-Johnstone criterion can extract a coherent vortex signal while leaving behind Gaussian random noise. We find that no threshold yields a strictly Gaussian incoherent component, and that the most Gaussian incoherent flow is found for data compression lower than that achieved with the fully iterated Donoho-Johnstone threshold. Moreover, even at such low compression, the incoherent component shows clear signs of large-scale spatial correlations that are signatures of the forcings used to drive the flows.

PACS numbers:

---

\* Corresponding author: mark.rast@lasp.colorado.edu

<sup>‡</sup> NCAR is sponsored by the National Science Foundation.

<sup>†</sup>Also, the University of California, Los Angeles, California.

<sup>§</sup>Also, the Geophysical Turbulence Program, NCAR

## I. INTRODUCTION

Previous work has explored the application of the discrete wavelet transform to two- and three-dimensional turbulence simulation data in an effort to segregate the flow into distinctly different components based on wavelet amplitudes (e.g. [1–3]). Farge et al. [1, 2] refer to this process as Coherent Vortex Extraction (CVE), reflecting the conjecture that turbulent flows are comprised of coherent structures that dominate at energy bearing scales and an incoherent background component which can be modeled as Gaussian random noise. Segregation relies on application of a wavelet amplitude threshold. The one generally employed is the universal threshold of Donoho and Johnstone [4]. This threshold is simple to employ and minimizes the maximum error in the signal in the presence of additive and uncorrelated Gaussian noise when the noise variance is known. As the noise variance is not known a priori for a turbulent flow, CVE relies on an iterative scheme [5] to estimate it.

Application of the CVE methodology has led to the identification of two apparent components in simulated turbulent flows: one reconstructed from a small percentage of the highest amplitude wavelet coefficients, called coherent and more generally considered signal, and the other reconstructed from the remaining coefficients, called incoherent and more generally considered noise [2]. The coherent component has properties similar to the original flow. It contains  $\sim 99\%$  of the kinetic energy of the unfiltered flow, has a relative kinetic helicity distribution  $h = \frac{\mathbf{u} \cdot \boldsymbol{\omega}}{|\mathbf{u}| |\boldsymbol{\omega}|}$  which peaks near  $\pm 1$ , as the original flow being examined, and shows a  $k^{-5/3}$  kinetic energy spectrum through the inertial range. The incoherent component, by contrast, typically contains less than 1% of the flow energy, shows a peak in its helicity distribution near  $h = 0$ , and exhibits a  $k^2$  kinetic energy spectrum [2, 3].

In this paper we report on the results of wavelet analysis of two  $1024^3$  simulations of turbulence forced coherently at large scale, one as a Taylor-Green and the other as an Arn’old-Beltrami-Childress (ABC) flow (Equations 3 and 4 below). We examine sensitivity to three different wavelets, apply threshold filtering to either the magnitude of the vorticity or the amplitudes of the individual components independently, and study compression ratios ranging from 10 to 98.7%, the later achieved when the iterative Donoho-Johnstone threshold is applied to the wavelet amplitudes of the individual vorticity components. We find, independent of the wavelet or thresholding scheme employed, that the gross properties of the coherent flow component are similar to those reported in previous CVE studies, and

additionally that it maintains the temporal correlations of the original flow. In contrast to previous work, however, we find that the incoherent flow component shows a  $k^2$  spectrum only when the threshold filter is applied to the individual vorticity components, not when it is applied to the vorticity magnitude as in previous studies, and when it occurs, the  $k^2$  scaling extends only over a small range of high wavenumbers. Moreover, although the incoherent flow displays short temporal correlation, as would be expected for random noise, the statistics at any single time are significantly non Gaussian. We examine this non Gaussianity for a range of filter thresholds and find that it persists to very low compression values. Further, we demonstrate that, even at low compression, the incoherent component shows spatial correlations which reflect the large-scale properties of the original flow and thus contains some residual signal that cannot be characterized as random noise.

This paper is organized as follows. In the next section we describe the forced Taylor-Green and ABC flow simulation solutions we analyze. In Section III we briefly summarize the CVE method as we apply it, and in IV present the results of that analysis. In Section V we look at the single-point statistics of the incoherent component more closely to determine if they are Gaussian, and examine the degree of Gaussianity as a function of compression. We also examine the point-wise helicity distributions to determine if important vector alignments are preserved. Finally, in Section VI we extend the analysis to include correlations within the flows to understand the spatial structure and temporal persistence of both the coherent and incoherent components, before concluding our discussion in Section VII.

## II. FORCED TURBULENCE SIMULATIONS

We examine two flows resulting from direct numerical simulation of the forced incompressible Navier-Stokes equations [6],

$$\partial_t \mathbf{u} + \mathbf{u} \cdot \nabla \mathbf{u} = -\nabla p + \nu \nabla^2 \mathbf{u} + \mathbf{f} \quad (1)$$

and

$$\nabla \cdot \mathbf{u} = 0, \quad (2)$$

where  $\mathbf{u}$  is the velocity,  $p$  the pressure,  $\nu$  the kinematic viscosity, and  $\mathbf{f}$  an applied specific body force. The equations are discretized pseudo-spectrally, employing 2/3 de-aliasing (maximum wavenumber  $k = k_{\max} = N/3$ ) [7] in a triply periodic domain with  $N = 1024$  grid

points in each of the three directions, and time advanced using a second order Runge-Kutta scheme. The resulting solutions are well resolved; the dissipative wavenumber is smaller than  $k_{\max}$  at all time steps. The product of  $k_{\max}$  and the Kolmogorov dissipation scale,  $\eta = (\nu^3/\epsilon)^{1/4}$  with  $\epsilon$  the energy injection rate, is 1.2 for both runs.

The simulations differ primarily in the body force applied. One employed a Taylor-Green form

$$\begin{aligned} \mathbf{f}_{TG} = f_0 & [\sin(k_F x) \cos(k_F y) \cos(k_F z) \hat{x} \\ & - \cos(k_F x) \sin(k_F y) \cos(k_F z) \hat{y}], \end{aligned} \quad (3)$$

with  $k_F = 2$  and a domain size of  $2\pi$ . Taylor-Green forcing does not introduce net kinetic helicity into the flow. The computed flow has an integral-scale Reynolds number of  $Re = 3950$  and a Taylor-scale Reynolds number of  $R_\lambda = 800$ .

The other implemented an Arn'old-Beltrami-Childress (ABC) form

$$\begin{aligned} \mathbf{f}_{ABC} = f_0 & \{ [B \cos(k_F y) + C \sin(k_F z)] \hat{x} \\ & + [A \sin(k_F x) + C \cos(k_F z)] \hat{y} \\ & + [A \cos(k_F x) + B \sin(k_F y)] \hat{z} \}, \end{aligned} \quad (4)$$

with  $k_F = 3$ , a domain size of  $2\pi$ ,  $A = 0.9$ ,  $B = 1$ , and  $C = 1.1$ . ABC forcing does introduce net positive helicity. The computed flow in this case has somewhat higher integral-scale and Taylor-scale Reynolds numbers,  $Re = 6200$  and  $R_\lambda = 1100$  respectively.

### III. COHERENT VORTEX EXTRACTION

We examine the simulation solutions using the multiresolution wavelet analysis and thresholding techniques of Farge et al. [1, 2, 5] to separate the flow based on its vorticity into the previously mentioned coherent (signal) and incoherent (noise) components. The CVE method consists of three steps [e.g. 8]:

1. Decomposition: An orthogonal wavelet transform of each vector component of the vorticity,  $\boldsymbol{\omega} \equiv [\omega_x, \omega_y, \omega_z]$ , yields the wavelet coefficient vector  $\tilde{\boldsymbol{\omega}}$ , the projection of the vorticity into wavelet space.

2. Thresholding: A filter is applied to the wavelet coefficients based on the magnitude of the vorticity vector. The threshold amplitude  $A_{DJ}$  is taken to be the “universal threshold” of [4],

$$A_{DJ} = \sqrt{\frac{4}{3}Z \ln N}, \quad (5)$$

where  $N$  is the total number of data points and  $Z \equiv \frac{1}{2} \langle \boldsymbol{\omega} \cdot \boldsymbol{\omega} \rangle$  is the enstrophy of the flow;  $Z/3$  is one-half the average variance of the three vorticity vector components when their means are zero. The incoherent (noise) component of the flow is then composed of those wavelet coefficient vectors with magnitude below the threshold value and the coherent (signal) component of those that exceed it. Since the universal threshold is defined in terms of the variance of the noise, and since the enstrophy of the incoherent vorticity (noise component) is not known a priori, Equation (5) is only a first estimate for the threshold value. It is refined iteratively [5] by successive evaluation of the variance of the incoherent component after filtering based on the previous threshold. The iteration converges when the variance of the incoherent vorticity becomes stationary; when there no change in the assignment of the coefficients as coherent or incoherent. This generally occurs after about 35 iterations.

Unlike previous work, we also examine a filtering scheme which employs the same filter threshold but applies it to each vorticity component separately and independently, based on their individual amplitudes. This iteratively converges to somewhat different results, primarily because it yields higher flow compression (Section IV), compressions more in line with those achieved by single iteration and applied to the vorticity magnitude [8–10].

3. Reconstruction: The coherent vorticity  $\boldsymbol{\omega}_C$  is reconstructed by the inverse wavelet transform of the wavelet vectors with magnitudes above the threshold value, or in the case of the filter being applied to the components, by the inverse transform of the wavelet coefficients with individual amplitudes that exceed the threshold value. Since the wavelets employed are orthonormal, the incoherent component  $\boldsymbol{\omega}_I$  can be reconstructed either by inverse transformation of the low magnitude wavelet vectors or low amplitude coefficients, or by subtracting the coherent component from the original vorticity;  $\boldsymbol{\omega}_I = \boldsymbol{\omega} - \boldsymbol{\omega}_C$ .

The data compression achieved by this process is defined as the fraction of coefficients used to construct the incoherent component, or equivalently the fraction considered noise and thus not needed in reconstruction of the signal (the coherent component approximation to the original flow).

Finally, the coherent and incoherent flow velocities are reconstructed from the corresponding vorticities via a spectral inverse curl. We note that the wavelet decomposition introduces signal above the Orszag frequency  $k_{\max}$  into both the coherent and incoherent components. The total power in the wavelet coefficients is preserved (incoherent and coherent contributions above  $k_{\max}$  sum to zero), but the spectra of the filtered components individually reflect this redistribution (Figure 3).

#### IV. CVE ANALYSIS OF TAYLOR-GREEN AND ABC FLOWS

The most important findings from previous CVE decompositions of turbulent flow are:

1. Using less than 2.6% of the wavelet coefficients in the reconstruction of the coherent vorticity yields a flow with nearly all (99.8%) of the kinetic energy and most of (79.8%) the enstrophy of the original flow [9].
2. The incoherent vorticity has low amplitude and is described as spatially random, structureless, and non-intermittent, though it displays an exponential distribution of values [2, 9, 11, 12]. The incoherent velocity is nearly Gaussianly distributed with very small variance [2, 9, 11, 12].
3. The relative kinetic helicity distribution of the incoherent component has the opposite curvature to that of the original, peaking near  $h = 0$  rather than at  $\pm 1$  as that of the original flow [2, 3, 12].
4. The kinetic energy spectrum of the coherent flow matches that of the original from the integral scale through the inertial range where it follows  $k^{-5/3}$ ; differences between the spectra are confined to the dissipative range. The incoherent component, on the other hand, shows  $k^2$  spectrum, with a peak at the low wave number end of the dissipative range where it joins the original flow spectrum [2, 3, 9, 12].

Forcing	Wavelet	Compression (%)		Kinetic Energy Retained (%)		Enstrophy Retained (%)	
		$ \boldsymbol{\omega} $	$ \omega_{x,y,z} $	$ \boldsymbol{\omega} $	$ \omega_{x,y,z} $	$ \boldsymbol{\omega} $	$ \omega_{x,y,z} $
Taylor-Green	Haar	94.5	98.6	98.8	97.2	90.4	80.8
Taylor-Green	Coifman12	91.8	97.6	99.98	99.8	98.1	94.9
Taylor-Green	Coifman30	91.3	97.4	99.99	99.9	98.7	96.1
Arn'old-Beltrami-Childress	Haar	94.6	98.7	99.1	97.9	89.7	79.8
Arn'old-Beltrami-Childress	Coifman12	92.0	97.7	99.97	99.9	97.9	94.4
Arn'old-Beltrami-Childress	Coifman30	91.4	97.4	99.99	99.9	98.5	95.7

TABLE I: Compression achieved and kinetic energy and enstrophy retained in the coherent component of the flow after employing the iterative Donoho-Johnstone filter threshold on two-flows with three wavelets. Results differ when application of the filter is based on the vorticity magnitude  $|\boldsymbol{\omega}|$  vs. component amplitudes  $|\omega_{x,y,z}|$ .

These findings largely result from Coifman12 wavelet analysis of both run-down and forced turbulent flows, though the results are reported to be robust to the choice of orthogonal wavelet, excluding the Haar [9], but not to biorthogonal decomposition [12]. Here we investigate the effectiveness of CVE when employing the Haar, Coifman12, and Coifman30 wavelets in the analysis of Taylor-Green and ABC flows.

The gross properties of our CVE results are similar to those previously published, but as summarized in Table I, the compressions we achieve when applying the iterative Donoho-Johnstone threshold to the vorticity vector magnitude are significantly lower than those previously reported in the literature. Consequently, our decompositions also show greater retention of the flow kinetic energy and enstrophy by the coherent component. This decreased compression is likely due to our using a fully iterated threshold value rather than that obtained by a single iteration as in most previous work [cf. 9]. We have applied single iteration thresholds and then obtain similar compressions (e.g. 97.3% using the Coifman 12 wavelet on the TG flow) to those published. We also obtain higher compression ratios, similar to those of previous single iteration studies, when we apply the full iterated threshold to individual vorticity component amplitudes rather than the vorticity vector magnitude. In those cases, the kinetic energy and enstrophy retained by the coherent flow are also reduced (Table I). For any of the threshold determination schemes, we find, as previous

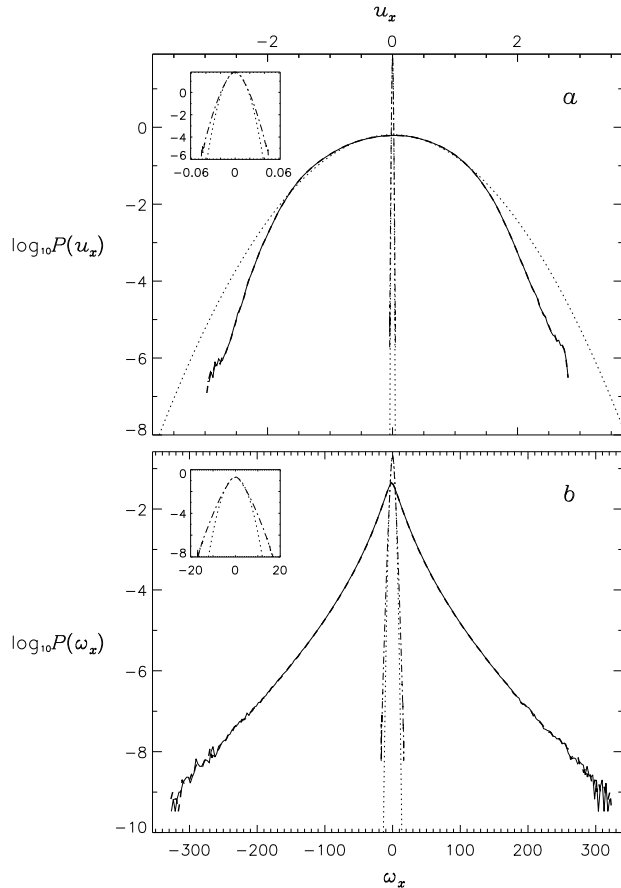


FIG. 1: Logarithm of the probability density of the velocity  $P(u_x)$  in (a) and vorticity  $P(\omega_x)$  in (b). The coherent (dashed) and incoherent (dot-dashed) components of the original (solid) Taylor-Green flow were computed using the Coifman12 wavelet in the CVE analysis (iterative Donoho-Johnstone threshold applied to vorticity magnitude). Dotted curves indicate Gaussian PDFs with the same mean and variance. Insets show incoherent flow velocity and vorticity PDFs and the Gaussian fits over a narrower range of values. The flow is quite isotropic with nearly identical PDFs for the  $y$  and  $z$  velocity and vorticity, though the  $z$  velocity is more Gaussian with somewhat smaller variance.

authors, that the gross properties of the coherent velocity and vorticity distributions are in good qualitative agreement with those of the unfiltered flow (Figure 1). We defer a quantitative assessment of the incoherent distributions to the next section (Section V). There we motivate even weaker compression of the signal than that achieved by application of the iterative Donoho-Johnstone threshold.

The detailed coherent and incoherent Taylor-Green and the ABC kinetic helicity and kinetic energy distributions are similarly sensitive to the filter threshold. While the original flows and their coherent components show relative helicity distributions similar to those reported in earlier studies when the flows are well resolved and have little mean strain [13–15], peaking weakly near  $h = \pm 1$ , the incoherent flow components typically display an helicity maximum near  $h = 0$  as in previous CVE studies (Figure 2). We note, however, that the incoherent ABC helicity distribution remains asymmetric, showing weak residual net helicity introduced by the forcing even at very low wavelet compression. Additionally, while the coherent flow kinetic energy spectra qualitatively match those of the original flows through the dissipative range and the incoherent power spectra peak at high  $k$  values (Figure 3), the later show the  $k^2$  scaling reported in previous CVE studies only when the filter is based on individual vorticity amplitudes rather than the vector magnitude, and even then over only a very limited range of wavenumbers. This again likely reflects the increased compression achieved in our work when the fully-iterated threshold is applied the vorticity vector components and in previous studies when a single iteration threshold is applied to the vorticity magnitude.

## V. A CLOSER LOOK AT THE ITERATIVE DONOHO-JOHNSTONE THRESHOLD

Separating a turbulent flow into coherent and incoherent components by wavelet transformation requires careful consideration of the threshold used in the filter operation. CVE estimates the variance of the noise as that of the vorticity and applies an iterative scheme [5] to estimate the universal threshold [4] based on convergence of the incoherent vorticity variance, though often that convergence is approximated by the variance after a single iteration [8–10] or the variance of the total vorticity itself (no iteration) [3, 16]. The fully iterated threshold would yield optimal de-noising if the flow vorticity were indeed composed of coherent signal and incoherent noise and if the later were both Gaussianly distributed and spatially uncorrelated. If such were the case, one would also expect the incoherent helicity distribution to reflect random velocity and vorticity vector orientations and the incoherent kinetic energy to scale as  $k^2$ .

### A. Is the incoherent vorticity Gaussianly distributed?

We tested the hypothesis that each vector component of the incoherent vorticity is independently Gaussianly distributed using the Pearson  $\chi^2$  and the Anderson-Darling tests [17–19]. We took the model distribution to be Gaussian with the same mean and variance as the incoherent data. To make the binned  $\chi^2$  test less sensitive to outliers, data that was further than  $\pm 4.5\sigma$  from the mean and thus corresponding to a model prediction of less than 5.5 points within the bin was excluded. The Anderson-Darling test is more robust to outliers and only values where the cumulative density function of the model Gaussian distribution had value zero or one to machine precision were omitted. Validation tests with  $1024^3$  Gaussianly distributed random numbers in place of the incoherent flow vorticity components confirmed with better than 99% confidence that in these test cases the hypothesis could not be dismissed. As a secondary validation criteria we confirmed that the probabilities-to-exceed in the random number cases were uniformly distributed.

We performed these tests on the incoherent vorticity identified using the iterative Donoho-Johnstone threshold applied to the vorticity magnitude (standard CVE analysis) in solutions with both flow forcings and employing all three wavelets. Both tests indicated that the incoherent flow vorticity is in all cases significantly non Gaussianly distributed. The  $\chi^2$  test yields zero probability-to-exceed to machine precision. The measured reduced  $\chi^2$  and the Anderson-Darling test statistic  $A^2$  ( $W_n^2$  in [18] and [19]) have values of  $\sim 1100$  and  $\sim 10^6$  respectively. The Gaussian distribution is rejected at the 1% significance level when these values exceed 1.02 and 1.09 for our binned  $\chi^2$  and Anderson-Darling tests respectively. We note that while the incoherent velocity appears by eye to be quite Gaussianly distributed, carefully evaluation indicates that it too shows non Gaussianity ( $\chi^2 \sim 300$  and  $A^2 \sim 5 \times 10^5$  respectively), though less than the incoherent vorticity. Here we focus on the Gaussianity of the incoherent vorticity because it is that quantity which underlies the applicability of the iterative Donoho-Johnstone threshold in CVE and CVS turbulence modeling.

Employing the same hypothesis tests, we examined a range of arbitrary wavelet amplitude thresholds. Compression near 80% yielded the most Gaussianly distributed (by either test) incoherent vorticity, with only weak sensitivity to the wavelet employed or the simulation solution studied (Figure 4a), though these most Gaussian distributions remain statistically non Gaussian with very large  $A^2$  values and zero probability-to-exceed reduced  $\chi^2$  values. We

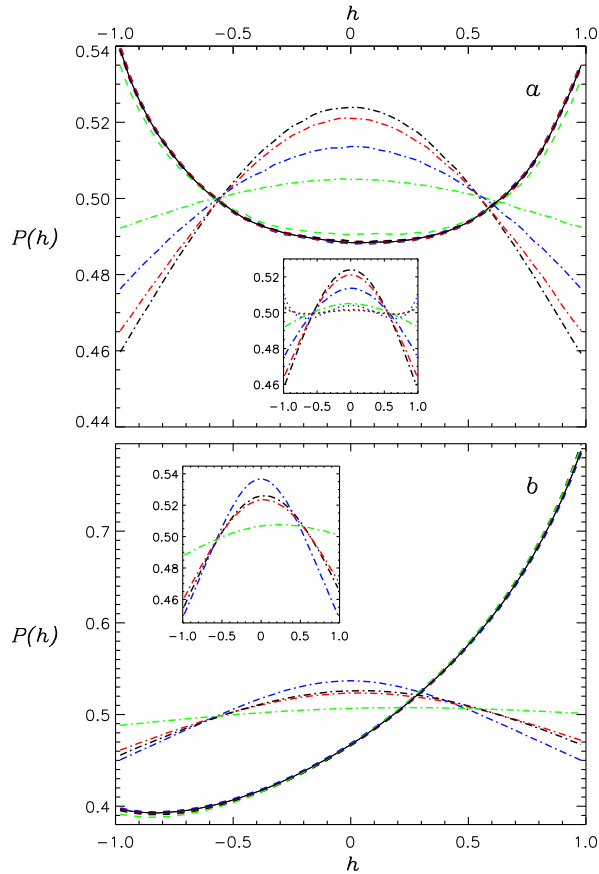


FIG. 2: Relative kinetic helicity distribution in the (a) Taylor-Green and (b) ABC flows. Black curves plot values for the original flow (solid) and the coherent (dashed) and incoherent (dot-dashed) components, the later found using the Coifman12 wavelet in the CVE analysis (iterative Donoho-Johnstone threshold applied to the vorticity vector magnitude). Red and blue curves show the same components obtained using the most Gaussian vorticity and 60% compression thresholds respectively. Green curves plot values obtained when applying the iterative Donoho-Johnstone threshold to individual vorticity component amplitudes. Insets display incoherent results over a limited range, and dotted curves in inset (a) indicate helicity distribution of randomized vector components (§VB).

also tested the Gaussianity of the incoherent distributions after thresholding the individual vorticity components rather than the vorticity vector magnitude. For any given compression rate, filtering the individual vorticity components yields more Gaussianly distributed (though still significantly non Gaussian) incoherent vorticity values than does filtering based on the vorticity vector magnitude. However, since, for a given threshold value, the overall

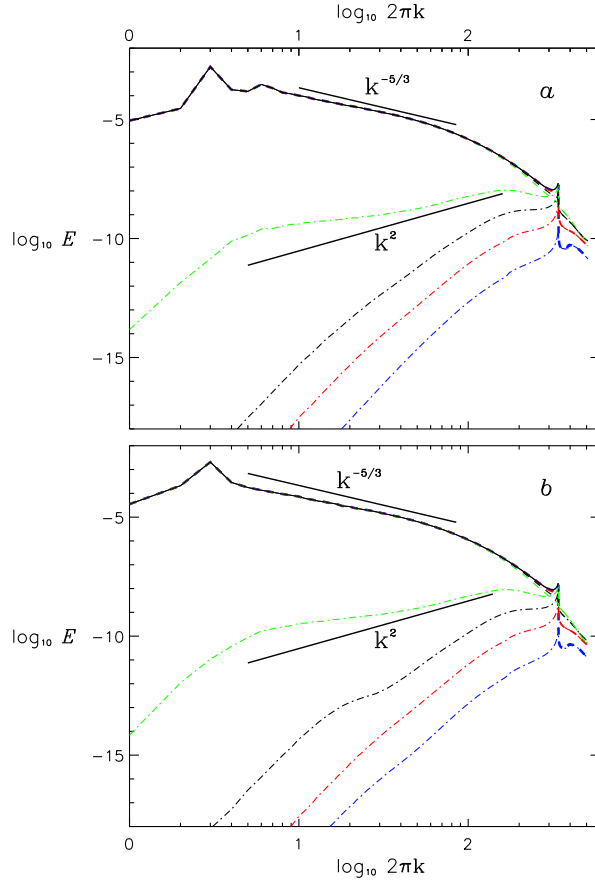


FIG. 3: Kinetic energy spectra of the (a) Taylor-Green and (b) ABC flows. Black curves for the original flow (solid) and coherent (dashed) and incoherent (dot-dashed) components, the later determined using the Coifman12 wavelet in the CVE analysis (iterative Donoho-Johnstone threshold applied to the vorticity vector magnitude). Red and blue curves show the same components obtained using the most Gaussian vorticity and 60% compression thresholds respectively. Green curves for values obtained by applying the iterative Donoho-Johnstone threshold to individual vorticity component amplitudes. Note that the wavelet decomposition introduces power above the Orszag frequency  $k_{\max}$  into both the coherent and incoherent components (§III), but that these sum to zero in amplitude. Fiducial  $k^{-5/3}$  and  $k^2$  lines shown for reference.

the compression is greater when the filter is based on vector component amplitudes than it is when based on vector magnitude, the Gaussianity of the incoherent vorticity is comparably less when the fully iterated threshold is applied to the vorticity vector components than when the same threshold is applied to the vector magnitude (Figure 4a).

We note that, while the Gaussianity of the incoherent flow monotonically increases with

decreasing compression down to 80%, it then somewhat counterintuitively decreases again from the minimum  $A^2$  value as even lower threshold values are employed (Figure 4). We understand this as follows: at very low compression ratios the incoherent vorticity component is composed of the few wavelets of lowest amplitude and its distribution is strongly peaked at zero since many nearly zero vorticity values contribute to the probability density. As the compression ratio increases and more wavelets are added to the incoherent component, the distribution “rounds out,” with wavelets of many scales randomly contributing. A minimum  $A^2$  value is reached, before, with further compression, the non Gaussian nature of the original vorticity distribution dominates the incoherent component, with the two becoming one and the same at 100% compression. Interestingly, and somewhat unexpectedly, near the most Gaussian value the curves collapse more completely when  $A^2$  is plotted against threshold value itself (Figure 4b) than when it is plotted against the compression achieved (Figure 4a). While the compression achieved for a given threshold depends on the details of wavelet employed, the Gaussianity of the noise seems to depend only on the threshold value itself.

### B. Does the incoherent flow helicity indicate random vector orientations?

The existence of a wavelet filter that yields a more Gaussianly distributed noise component than that found via the iterative Donoho-Johnstone scheme, suggests that the conditions necessary for the successful application of the universal threshold may not be met in these turbulence simulation solutions, that the two component decomposition fails because the incoherent component is both non Gaussian and retains correlations which persist to very low amplitudes in the turbulent flow.

Figure 2a shows that the kinetic helicity distribution of the incoherent component of the Taylor-Green flow peaks at  $h = 0$  and has opposite curvature to that of the original, as it also does in previous work [2, 3, 12]. Vectors of random magnitude and orientation would show uniformly distributed helicity (with normalized  $P(h) = 0.5$ ). The incoherent helicity distribution differs from this, though scrambling the individual incoherent vorticity and velocity vectors by randomly sampling their components produces helicity distributions that are close to uniform (dotted curves in inset of Figure 2a) indicating that it is the helicity vector direction that is to some degree preserved by the incoherent flow. Thus, application of the threshold filter to individual vorticity component amplitudes rather than the vector

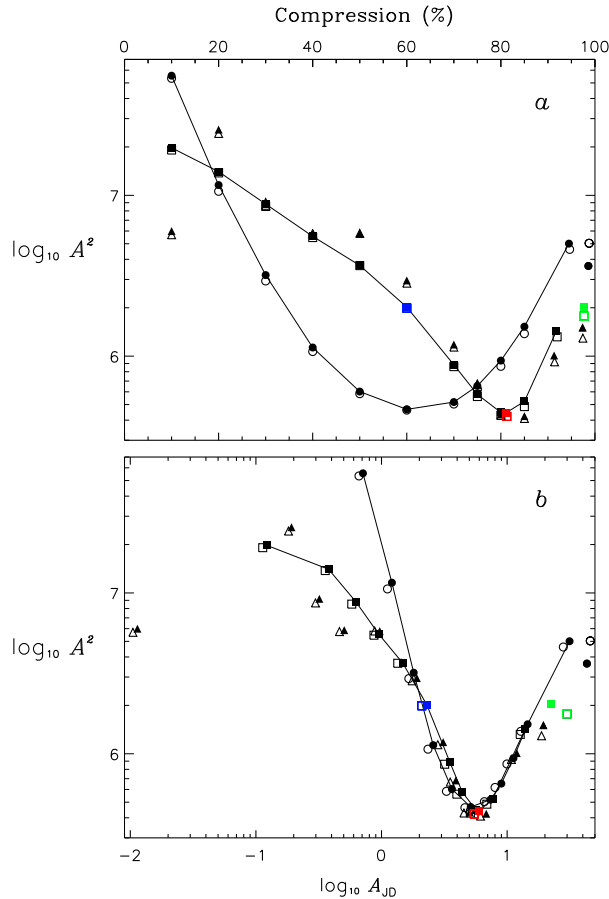


FIG. 4: In (4a), the Anderson-Darling test statistic  $A^2$  measuring the Gaussianity of the incoherent component of the flow as a function of compression, and in (b)  $A^2$  as a function of threshold value  $A_{DJ}$ . Filled and empty symbols indicate analysis on the Taylor-Green and ABC solutions respectively. The incoherent component was extracted using the Haar (circles), Coifman12 (squares), and Coifman30 (triangles) wavelets. The threshold yielding the most Gaussian incoherent component with the Coifman12 wavelet is shown in red and that yielding 60% compression in blue (60% compression symbols for Taylor-Green and ABC flows directly overlap). The incoherent  $A^2$  values obtained using the iterative Donoho-Johnstone threshold applied to the individual vorticity amplitudes are those with the highest compression, with those employing the Coifman12 wavelet shown in green. Colors correspond to those in all figures. Black curves highlight Coifman12 and Haar analysis of the Taylor-Green flow.

magnitude yields an incoherent helicity distribution closest to that of randomly oriented vectors because such component filtering serves to scramble the vorticity and velocity vector directions. Without such scrambling, as when the threshold filter is applied to the vorticity vector magnitudes (the usual CVE procedure), a residual of the original flow helicity

contaminates in the incoherent component. This is true for all filter thresholds, with no wavelet decomposition of the Taylor-Green flow yielding strictly randomly oriented vorticity and velocity vectors, and a consequent uniform helicity distribution, in the incoherent flow. Analysis of the ABC flow (Figure 2b) confirms this result. Net helicity is introduced into the ABC flow via the driving, and the incoherent component in all cases reflects this bias, albeit very weakly at 60% compression.

### C. Does the incoherent kinetic energy scale as $k^2$ ?

A spatially uncorrelated three-dimensional random field (equal power in all spectral modes independent of direction) necessitates power scaling as  $k^2$ . This scaling is reported for the incoherent flow component of previously published wavelet decompositions [2, 3, 9, 12]. We find it to hold only over a very limited range of high wavenumbers and then only when the each component of the vorticity is filtered independently, not when the filtering is applied to the vorticity vector magnitude, though it is the later procedure which is followed in previous studies. In our studies, filtering by the vorticity vector magnitude yields much steeper incoherent kinetic energy spectra (Figure 3). This likely results because, it is only by filtering the vorticity components separately that we achieve compression rates comparable to those previously published, and it is this overall compression that largely determines low wavenumber contributions to the incoherent component. We have computed the single iteration incoherent energy spectra for both the TG and ABC flows and these show flatter spectra, akin to those reported by previous authors, though some uncertainty remains as published fully iterated results do not show the steeper slope that we find [cf. 9].

The simulations studied here were force coherently, with turbulence developing from the instability of the large-scale flow driven with a well defined geometry. The steeper incoherent power spectrum observed in our work may reflect the coherent nature of our low wave number driving, with that coherence partially destroyed when the filter is applied to individual component amplitudes, flattening the noise spectrum toward  $k^2$ . However, we note that previous CVE studies which also show the flatter spectrum examined both run-down and forced turbulence simulation solutions resulting from a range for forcing schemes. It is thus likely that it is the high compressions achieved in those studies and in our component filtering analysis, rather than the particulars of the flow forcing, that underly the enhanced

low wavenumber power spectrum observed. It is unclear, therefore, whether the limited  $k^2$  spectra observed necessarily implies the existence of a spatially uncorrelated random component in the flow.

## VI. SPATIAL AND TEMPORAL CORRELATIONS

The coherence of our driving scheme is also reflected in persistent spatial correlations evident in the incoherent component of the Taylor-Green and ABC flows even at very low compressions. As an example, the Taylor-Green forcing (Equation 3) has a cosine form in the  $z$  direction, with alternating regions of oppositely signed forcing producing regions of high vorticity at the interfaces. The autocorrelation of the enstrophy in that direction shows these alternating regions clearly in both the coherent and incoherent components (Figure 5a). In fact, when employing the iterative Donoho-Johnstone threshold the large scale correlations have a larger amplitude in the incoherent flow component than they do in the original flow because smaller scale fluctuations contribute less to the correlation measure. At lower compressions the signature of the large scale forcing is reduced but persists. We note that the spatial autocorrelation plot in Figure 5a shows two curves for each of the incoherent components. This reflects oscillations in the incoherent component at the Nyquist frequency, not seen in the original flow, due to enhanced power above the Orszag frequency  $k_{\max}$  as a result of the wavelet filtering (see §III).

Understanding the temporal correlation of the incoherent component is important to efforts aimed at using CVE filtering and incoherent component modeling as simulation tools. We find such temporal correlations to be less pronounced than the spatial correlations. We computed the temporal correlation of one vorticity component between 40 volumetric snapshots spanning 0.4 turnover times of the Taylor-Green flow (the turnover time here defined in terms of the integral length scale and the root-mean-square velocity). The iterative Donoho-Johnstone filter threshold was vary stable over these snapshots. The number of iterations required for convergence varied between 32 and 38, and the threshold values differed by at most 1.3% between any two snapshots. A full width half maximum de-correlation time of  $\sim 0.056$  was found for both the original flow and coherent component while one of  $\lesssim 0.01$  was obtained for the incoherent component. Slightly shorter temporal correlation times were found for lower compressions, but even the iterative Donoho-Johnstone scheme applied to

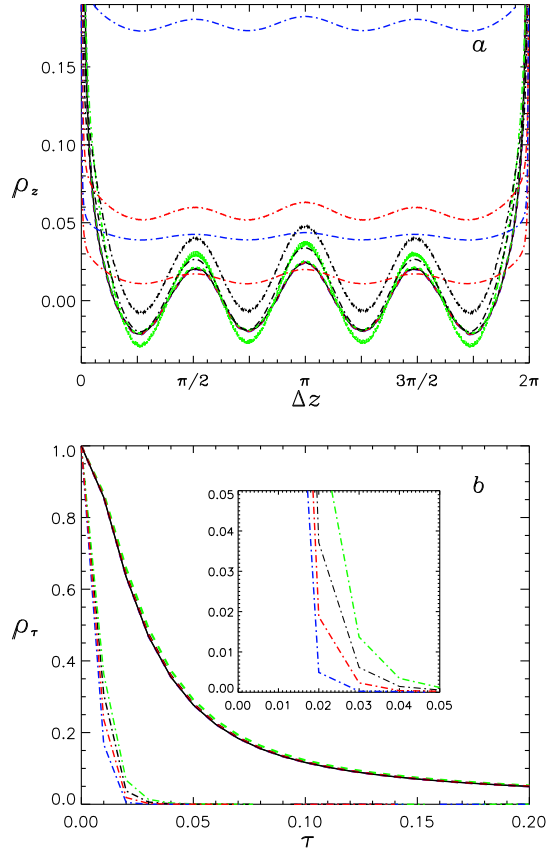


FIG. 5: In (a), spatial autocorrelation  $\rho_z$  of the Taylor-Green enstrophy as a function of the spatial lag  $\Delta z$ , and in (b), the temporal correlation  $\rho_\tau$  of Taylor-Green vorticity  $\omega_x$  as a function of temporal lag  $\tau$  (vorticity chosen here only to reduce the computational cost of time series analysis). Black curves for the original flow (solid) and coherent (dashed) and incoherent (dot-dashed) components, the later determined using the Coifman12 wavelet in the CVE analysis (iterative Donoho-Johnstone threshold applied to the vorticity vector magnitude). Red and blue curves show the same components obtained using the most Gaussian vorticity and 60% compression thresholds respectively. The iterative Donoho-Johnstone threshold applied to the individual vorticity amplitudes is shown in green. The coherent components (dashed lines) in (a) underlie the solid curve and are thus hidden from view. The double curve for each of the incoherent components (dot-dashed lines) in (a) reflects grid oscillation of the incoherent component at the Nyquist frequency, not seen in the original flow, due to enhanced power above the Orszag frequency  $k_{\max}$  as a result of the wavelet filtering (§III).

the individual vorticity amplitudes (maximum compression) yielded an incoherent flow with very short temporal correlation (Figure 5b).

## VII. CONCLUSION

Wavelet filtering promises significant compression of turbulence simulation data and possible modeling schemes based on evolving the coherent flow component only. The coherent flow identified in the CVE analysis shares many properties with the original solutions using only a small fraction of the wavelet coefficients. A scheme which evolves these coefficients while modeling the remaining incoherent contribution would yield a tremendous decrease in computation effort [16]. The difficulty lies in how best to model the incoherent or noise component.

Our results suggest that the incoherent component of forced turbulence, when extracted using an orthonormal wavelet decomposition, cannot be strictly modeled as Gaussian random noise. It retains residual vector correlations (helicity) found in the original flow and spectral energy distribution and spatial correlations that reflect the forcing function. These difficulties can be diminished by reducing the threshold criterion, thereby reducing the compression achieved, but they persist at some level for all thresholds we examined. The turbulent flows we examined (forced coherently at large scale as a Taylor-Green or Arn'old-Beltrami-Childress (ABC) flow) cannot be conceptually separated into coherent signal and incoherent noise with distinctly different properties. The filtering operation always to some extent removes flow in addition to any noise component that may be present. The short temporal correlation time of the incoherent component does however suggest that if, despite these difficulties, a model of the low amplitude coefficients can be developed, that model could be based on the current state of the coherent flow, independent of its evolution.

Another item of significant interest to modeling efforts is the flow divergence introduced by CVE filtering. We found that ???. Careful study of the sensitivity of this result to the wavelet type, filtering scheme, and compression achieved is left for future study.

---

[1] M. Farge, K. Schneider, and N. Kevlahan. Non-gaussianity and coherent vortex simulation for two-dimensional turbulence using an adaptive orthogonal wavelet basis. *Physics of Fluids*,

- 11(8):2187–2201, 1999.
- [2] M. Farge, G. Pellegrino, and K. Schneider. Coherent Vortex Extraction in 3D Turbulent Flows Using Orthogonal Wavelets. *Physical Review Letters*, 87(5):054501, 2001.
- [3] B. Kadoch, M. Oliveira Domingues, I. Broemstrup, L. Larchevêque, K. Schneider, and M. Farge. Coherent Vorticity Extraction in 3D Homogeneous Isotropic Turbulence: Influence of the Reynolds Number and Geometrical Statistics. *Brazilian Journal of Physics*, 39(2):531–538, 2009.
- [4] D. L. Donoho and I. M. Johnstone. Ideal spatial adaptation by wavelet shrinkage. *Biometrika*, 81(3):425–455, 1994.
- [5] A. Azzalini, M. Farge, and K. Schneider. Nonlinear wavelet thresholding: A recursive method to determine the optimal denoising threshold. *Applied and Computational Harmonic Analysis. Elsevier*, 18:177–185, 2005.
- [6] P. D. Mininni, A. Alexakis, and A. Pouquet. Large-scale flow effects, energy transfer, and self-similarity on turbulence. *Phys. Rev. E*, 74(1):016303, 2006.
- [7] S. A. Orszag. On the elimination of aliasing in finite-difference schemes by filtering high-wavenumber components. *Journal of the Atmospheric Sciences*, 28(6):1074–1074, 1971.
- [8] F. Jacobitz, L. Liechtenstein, K. Schneider, and M. Farge. On the structure and dynamics of sheared and rotating turbulence: Direct numerical simulation and wavelet-based coherent vortex extraction. *Physics of Fluids*, 20(4):045103, 2008.
- [9] N. Okamoto, K. Yoshimatsu, K. Schneider, M. Farge, and Y. Kaneda. Coherent vortices in high resolution direct numerical simulation of homogeneous isotropic turbulence: A wavelet viewpoint. *Physics of Fluids*, 19(11):115109, 2007.
- [10] N. Okamoto, K. Yoshimatsu, K. Schneider, M. Farge, and Y. Kaneda. Coherent vorticity simulation of three-dimensional forced homogeneous isotropic turbulence. *Multiscale Modeling and Simulation*, 9(3):1144–1161, 2011.
- [11] M. Farge, K. Schneider, G. Pellegrino, A. A. Wray, and R. S. Rogallo. Coherent vortex extraction in three-dimensional homogeneous turbulence: Comparison between CVS-wavelet and POD-Fourier decompositions. *Physics of Fluids*, 15(10):2886–2896, 2003.
- [12] O. Roussel, K. Schneider, and M. Farge. Coherent vortex extraction in 3D homogeneous turbulence: Comparison between orthogonal and biorthogonal wavelet decomposition. *Journal of Turbulence*, 6(11), 2005.

- [13] M. M. Rogers and P. Moin. Helicity fluctuations in incompressible turbulent flows. *Physics of Fluids*, 30(9):2662–2671, 1987.
- [14] R. M. Kerr. Histograms of helicity and strain in numerical turbulence. *Physical Review Letters*, 59(7):783–786, 1987.
- [15] A. Tsinober, E. Kit, and T. Dracos. Experimental investigation of the field of velocity gradients in turbulent flows. *Journal of Fluid Mechanics*, 242:169–192, 1992.
- [16] K. Schneider, M. Farge, G. Pellegrino, and M. M. Rogers. Coherent vortex simulation of three-dimensional turbulent mixing layers using orthogonal wavelets. *Journal of Fluid Mechanics*, 534:39–66, 2005.
- [17] K. Pearson. On the criterion that a given system of deviations from the probable in the case of a correlated system of variables is such that it can be reasonably supposed to have arisen from random sampling. *Philosophical Magazine*, 50(302):157–175, 1900.
- [18] T. W. Anderson and D. A. Darling. Asymptotic theory of certain ‘goodness of fit’ criteria based on stochastic processes. *Annals of Mathematical Statistics*, 23(2):193–212, 1952.
- [19] T. W. Anderson and D. A. Darling. A test of goodness of fit. *Journal of the American Statistical Association*, 49(268):765–769, 1954.

### **Acknowledgments**

Special thanks to J.-F. Pinton, A. Pouquet, and an anonymous referee. CM thanks the NCAR SIParCS Program and JWL thanks the Graduate School of the University of Colorado for their generous support.